

Chemical Science

Accepted Manuscript

This article can be cited before page numbers have been issued, to do this please use: K. A. Yadav, G. Mishra, S. Kundu, S. Ghosh and R. Haldar, *Chem. Sci.*, 2025, DOI: 10.1039/D5SC04618A.



This is an Accepted Manuscript, which has been through the Royal Society of Chemistry peer review process and has been accepted for publication.

Accepted Manuscripts are published online shortly after acceptance, before technical editing, formatting and proof reading. Using this free service, authors can make their results available to the community, in citable form, before we publish the edited article. We will replace this Accepted Manuscript with the edited and formatted Advance Article as soon as it is available.

You can find more information about Accepted Manuscripts in the [Information for Authors](#).

Please note that technical editing may introduce minor changes to the text and/or graphics, which may alter content. The journal's standard [Terms & Conditions](#) and the [Ethical guidelines](#) still apply. In no event shall the Royal Society of Chemistry be held responsible for any errors or omissions in this Accepted Manuscript or any consequences arising from the use of any information it contains.

ARTICLE

Spatial functionality gradient in ZIF-8 thin film membrane

KM. Archana Yadav^a, Girish Mishra^{a†}, Susmita Kundu^{a‡}, Soumya Ghosh^a and Ritesh Haldar^{*a}[†]Received 00th January 20xx,
Accepted 00th January 20xx

DOI: 10.1039/x0xx00000x

Zeolitic Imidazolate Framework-8 (ZIF-8), constructed from Zn^{2+} ions and 2-methylimidazole (mIm) linkers, is widely recognized for its excellent thermal and chemical stability, making it a strong candidate for chemical separation and heterogeneous catalysis. In this study, we report a new crystalline phase of functionalized ZIF-8 featuring a spatially graded distribution of chemical functionality. This anisotropic functionalization is achieved via a vapor-phase process applied to a ZIF-8 monolithic film. Anisotropic diffusion of a reactive linker—imidazole-2-carboxaldehyde (CHO-Im)—into the ZIF-8 monolith results in a gradient incorporation of CHO-Im, yielding a ZIF-8-CHO monolith. Spatial anisotropy of the CHO functional groups is confirmed through X-ray diffraction, scanning electron microscopy, and vibrational spectroscopy. To demonstrate its potential, we fabricated an anodic aluminium oxide-supported membrane and highlighted its enhanced gas permselectivity compared to pristine membrane.

Introduction

Porous materials with tunable pore structures and chemical functionalities are highly sought after for the development of advanced chemical separation technologies (membranes). Among the contemporary materials, metal-organic frameworks (MOFs) stand out due to their exceptional chemical modularity, enabling the tailored design of materials for specific applications. Some of the MOFs (zeolitic imidazolate frameworks, Zr-based MOFs and others) have been extensively investigated for gas storage, molecular separation, catalysis, selective ion conduction, and beyond. Over the past two decades, a vast array of MOF structures with diverse and specialized chemical characteristics has been discovered. A notable advancement in this field is the development of mixed-component, or multivariate materials that incorporate multiple organic linkers or metal nodes in controlled ratios to generate synergistic and emergent properties (enhanced selectivity,² adsorption,^{3, 4} diffusion,^{5, 6} excitation energy transfer,⁷⁻⁹ electron-hole separation,¹⁰ catalysis¹¹). While these mixed-component systems have shown considerable promise in enhancing adsorption selectivity¹² (CO_2 under humid condition,² CH_4 adsorption,³ H_2 adsorption⁴), precise spatial control over the distribution of chemical functionalities remains a significant challenge.^{4, 13, 14} In polycrystalline MOF powders, mixed-linker strategies are relatively well-established¹⁴ (for

example, spatial distribution modulation in core-shell type crystals)¹⁵; however, translating this approach to device-relevant architectures such as thin films presents even greater technical hurdles.

Zeolitic imidazolate frameworks (ZIFs),¹⁶⁻¹⁸ a prominent subclass of MOFs, have been extensively investigated for their potential in chemical separations,¹⁷ owing to their excellent chemical stability and functional versatility.¹⁶ The incorporation of multiple linkers in ZIFs—through mixed-linker strategies—has been particularly successful, enabling fine-tuning of their properties.¹⁹⁻²¹ Moreover, ZIFs have been fabricated into thin-film membranes, and functional heterostructures composed of ZIFs have been realized. Prior studies have consistently demonstrated that such heterostructures yield enhanced performance, which has been attributed to the presence of chemically distinct interfaces (e.g., in core-shell architectures and bilayer films) and the cooperative behaviour of multiple linkers in mixed-linker systems. In the present study, we move beyond the traditional strategies of creating discrete interfaces or uniformly mixing chemical functionalities. We demonstrate that spatially gradient chemical functionality within ZIFs—specifically within the ZIF-8 structure is feasible and this feature can tailor the molecular sieving property. Scheme 1 illustrates a spatial functional gradient in a MOF monolith, in contrast to the conventional mixed-linker and MOF-on-MOF heterostructure. In this study, we applied the concept of a spatial chemical functionality gradient to a monolithic film of ZIF-8, constructed by linking Zn^{2+} and 2-methylimidazole (mIm). Specifically, a –CHO functionalized imidazole linker (CHO-Im) was gradiently distributed within the ZIF-8 monolith using a vapor-phase linker exchange reaction.

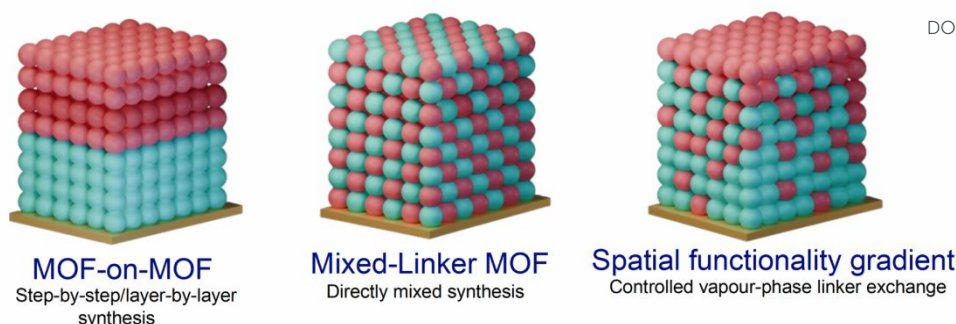
^a Tata Institute of Fundamental Research Hyderabad, Gopanpally 500046 Hyderabad, India.

Email: riteshhaldar@tifrh.res.in

[†] Footnotes relating to the title and/or authors should appear here.

Electronic Supplementary Information (ESI) available: [details of any supplementary information available should be included here]. See DOI: 10.1039/x0xx00000x





Scheme 1: A schematic illustration of mixed-linker MOF structures with different possible spatial configuration and fabrication methods; left to right: MOF-on-MOF, homogenously mixed-linker and the spatial gradient, which is demonstrated in the current work. Two differently colored spheres are used to represent different linker's presence in the MOF.

Our investigation aimed to demonstrate the feasibility of creating such a chemical functionality gradient within the thin film of ZIF-8. The results revealed the formation of a unique mixed-linker ZIF-8 monolith, but not a ZIF-8/ZIF-90 mixed crystalline phase film (ZIF-90 is made of Zn^{2+} and CHO-Im). In the monolith structure, CHO-Im was distributed according to a diffusion gradient leveraged by the vapor-phase reaction. This spatial distribution gradient significantly enhanced the molecular sieving properties of the material. Here, we detail the principle and methodology used to achieve this spatial gradient functionality in ZIF-8 and reveal its distinctive properties.

Result and discussion

Vapour-phase ZIF-8 functionalization

ZIF-8 exhibits a sodalite topology characterized by distinct hexagonal pore windows approximately 3.4 Å in diameter¹. While the Zn^{2+} -N coordination bonds in ZIF-8 are chemically stable, their reversible nature permits linker-exchange reactions. As a result, the 2-methylimidazole (mIm) linkers in ZIF-8 can be partially or fully replaced with other substituted imidazoles, enabling the synthesis of new ZIFs or mixed-linker variants. This exchange can be achieved through solvent-assisted methods or vapor-phase reactions, as demonstrated in previous studies²²⁻²⁶. An alternative approach involves the direct incorporation of additional imidazole-based linkers alongside mIm during synthesis to produce mixed-linker ZIFs. It is important to note that such linker mixing strategies have been predominantly explored in polycrystalline powder ZIF-8, often yielding structurally distinct ZIF phases^{22, 27, 28}. In powder ZIFs, the isotropic diffusion of linkers into the particles facilitates the formation of new ZIF structures, as reported in earlier literature²⁹⁻³¹. In some cases, slow linker diffusion can lead to the development of core-shell-type heterostructures³²⁻³⁴. Another theoretically possible outcome is a gradient distribution of the exchanging linker; however, such configurations have not been reported. This absence is likely due to the broad distribution of crystallite sizes in powders, which results in variable diffusion rates and renders the identification of a gradient phase challenging. Moreover, the functional impact of such a gradient distribution is difficult to evaluate in powder samples of ZIFs or other MOFs. In the

present study, we aim to investigate the feasibility and functional implications of gradient linker distributions within ZIF-8 structures.

In this study, we employed a vapor-phase linker exchange strategy on ZIF-8 monolithic thin films to investigate the feasibility of achieving gradient functional conversion, as depicted in Scheme 1. The choice of a monolithic thin film was intentional, as it facilitates anisotropic linker diffusion along the film's thickness, thereby providing a suitable platform to explore spatial variations in composition. Under conditions of uniform and efficient linker exchange, a complete transformation from ZIF-8 to ZIF-90 would be anticipated using 2-carboxaldehyde imidazole (CHO-Im) as the exchanging linker. However, other outcomes are also possible, such as the formation of a homogeneous ZIF-8_ZIF-90 mixture or a spatially graded composite of the two (Figure S1). In the sections that follow, we detail the synthesis methodology and provide evidence that the vapor-phase exchange results in a spatial gradient of CHO-Im incorporation. Rather than yielding a simple mixture or full conversion, the process gives rise to a CHO-Im functionalized ZIF-8 structure—hereafter referred to as ZIF-8-CHO (Figure 1a). We further demonstrate that this spatially graded monolith exhibits enhanced molecular sieving performance, underscoring the significance of gradient linker distribution in tuning material properties.

We have firstly synthesized a ZIF-8 monolithic film on -OH functionalized Au substrates using a previously established solution phase layer-by-layer methodology³⁵ (see supporting information for experimental details). The grown thin film exhibited sharp diffraction peaks corresponding to phase-pure ZIF-8 (Figure 1b). To introduce a new linker in this ZIF-8 film, we have adopted a vapour-phase linker exchange reaction. Firstly, the ZIF-8 film was activated and then placed in a closed glass chamber loaded with CHO-Im for 72 h at 353 K. After cooling down to room temperature, the modified film was washed thoroughly using dichloromethane and dried under vacuum at 323 K for 12 h. The purpose of thorough cleaning was to ensure the removal of unreacted and trapped linkers. The treated film was then examined by XRD, infrared reflection absorption spectroscopy and SEM (Figure 1b-e). The vapour phase treatment can give rise four possible structures: I) fully converted ZIF-90, II) ZIF-8/ZIF-90 mixed phases, III) ZIF-8_ZIF-90



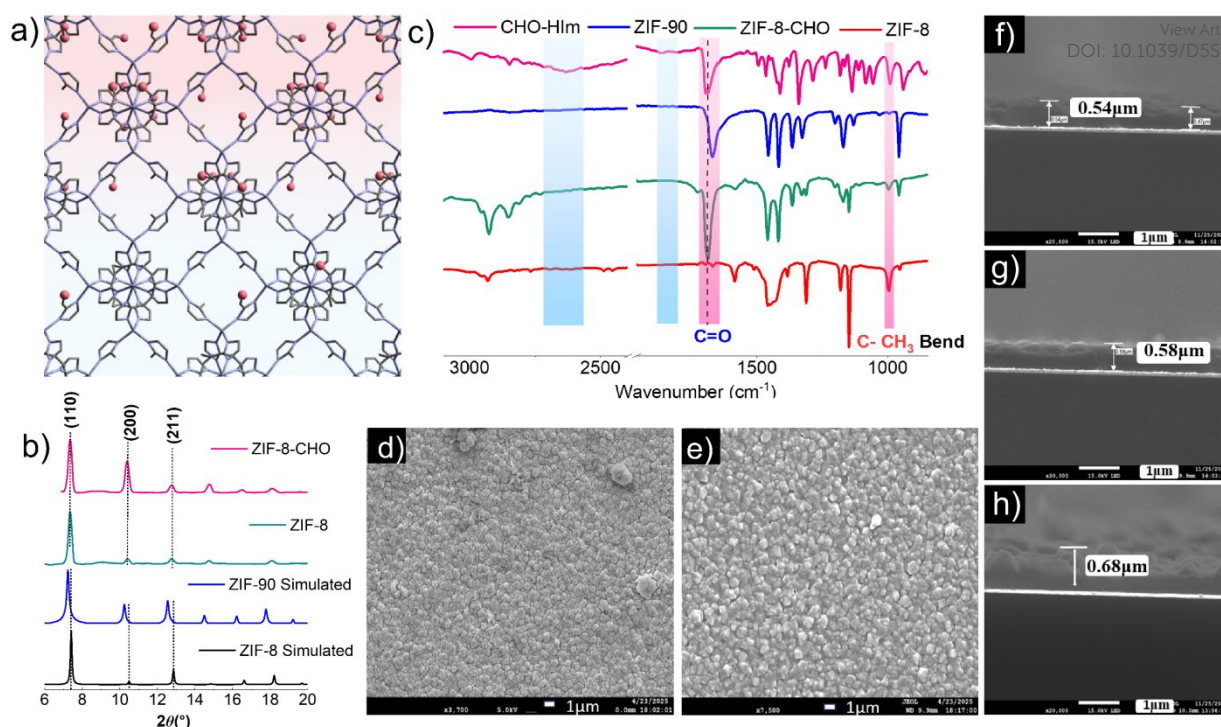


Figure 1. a) Illustration of ZIF-8-CHO hetrostructure thin film (red sphere = CHO group) b) Out-of-plane XRD patterns of ZIF-8-CHO and ZIF-8 with simulated ZIF-8 and ZIF-90 c) IRRAS of the ZIF-8-CHO, ZIF-8, ZIF-90(powder), 2-Imidazolecarboxaldehyde(powder) d-e) SEM morphology of ZIF-8 and ZIF-8-CHO f-g-h) Cross-section SEM images of ZIF-8, ZIF-8-CHO, ZIF-8_ZIF-90, respectively.

bilayer structure and IV) spatial gradient of CHO-Im functionalization in ZIF-8. Cases II-IV are illustrated in Figure S1. The main difference between II and IV is the distribution of CHO-Im linkers. Case iii may arise, if top ZIF-90 layer acts as a barrier to CHO-Im diffusion. The XRD pattern of the 72 h modified film (ZIF-8-CHO) exhibited a very similar pattern like for parent ZIF-8 (Figure 1b). Note, a time dependent study confirmed 72 h needed for the conversion (see Figure S2). This XRD data confirmed that the lattice dimension did not change by the vapour-phase reaction. However, the intensity ratio of the peaks corresponding to (110) and (200) plane changed substantially after the vapour phase reaction. Note that ZIF-8 and ZIF-90 unit cell dimensions differs by a small amount, and the crystal symmetry is same. An earlier investigation of mixed-linker ZIF indicated that the unit cell dimensions do not differ in

the mixed-phase¹⁹. Hence, we assumed that ZIF-90 conversion is possibly successful.

To confirm the presence of CHO-Im, we have carried out IRRAS experiments (Figure 1c). The ZIF-8-CHO film exhibited a strong absorption at 1685 cm^{-1} corresponding to C=O stretching vibration. This feature is missing in parent ZIF-8 structure. Few additional features are: i) C-CH₃ bending mode at 995 cm^{-1} is present in ZIF-8-CHO, confirming presence of ZIF-8, ii) absence of free -NH modes (1848 , 1820 , and $2400\text{--}3200\text{ cm}^{-1}$) in ZIF-8-CHO confirmed that unreacted CHO-Im is absent, and iii) C=O stretching frequency in ZIF-8-CHO at 1685 cm^{-1} is different than that in neat ZIF-90 (1670 cm^{-1}). These above observations rule out the possibility of case i type structure. Most striking revelation was the unique C=O stretching mode. In the absence of noncoordinated CHO-Im, we can attribute the shift in C=O mode to a lattice constrain (vide infra). Note that the observed C=O stretching did not arise because of incomplete reaction, as can be seen from reaction time-dependent IRRAS (Figure S2). At shorter time scale, C=O stretching at 1685 cm^{-1} is very weak and intensity enhances at longer time of exchange reaction (1683 cm^{-1}).

Figure 1d-e clearly indicated that the ZIF-8 and ZIF-8-CHO thin films are homogenous continuously grown, thus avoiding formation of island type structure. This homogeneity is more evident in Figure 1f-g, which shows the cross-section SEM view. Vapour-phase conversion did not change the film thickness. On the contrary, a solvothermal growth of ZIF-90 on top of ZIF-8 did change the film thickness (Figure 1h, the synthesis of bilayer ZIF-8_ZIF-90 is discussed in the supporting information).

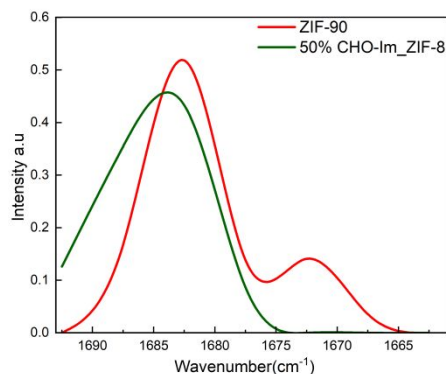


Figure 2. DFT calculated IR frequency plots of ZIF-90 and 50% CHO-Im in ZIF-8.



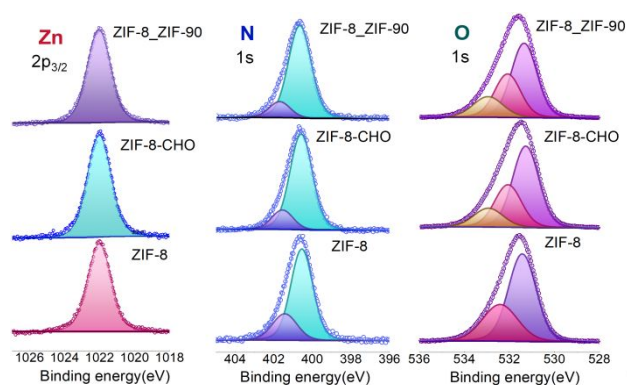


Figure 3. The XPS spectra of ZIF-8, ZIF-8-CHO and ZIF-8_ZIF-90 for Zn, N, O.

To confirm that the unique C=O stretching frequency is indeed due to lattice constrain, we have calculated (density functional theory) and compared the C=O vibration of neat ZIF-90 and a 50% doped CHO-Im in ZIF-8 lattice (see computational details in the supporting information). In Figure 2, it is evident that the C=O vibration frequencies are shifted to higher wavenumber, as observed in the experiment.

Next, x-ray photoelectron spectroscopy (XPS) was performed to evaluate chemical conversion of the ZIF-8 thin film (Figure 3). Note that the XPS data mostly provide information of the top ~10 nm of the thin film. The Zn 2p_{3/2} core-level spectra exhibited a gradual increase in binding energy from 1022.0139 eV in pristine ZIF-8 to 1022.023 eV in ZIF-8-CHO. This binding energy increment indicates modifications in the local coordination environment of zinc, likely due to the introduction of electron-withdrawing aldehyde functionalities. The N 1s spectra revealed two components corresponding to N–H and N–Zn bonding. In ZIF-8, these peaks were observed at 401.435 eV and 400.549 eV, respectively. In ZIF-8-CHO, the binding energies shifted to 401.5583 eV (N–H) and 400.5845 eV (N–Zn), attributed to the electronic effects of the CHO substituents. The O 1s spectra also showed significant changes consistent with functional group variation. For ZIF-8, the Zn–O and O–H components appeared at 532.416 eV and 531.435 eV, respectively. Upon functionalization to ZIF-8-CHO, the O 1s spectrum showed three components: Zn–O at 532.0860 eV, OH/MeOH at 531.2939 eV, and a C=O peak at 532.9602 eV, indicating successful incorporation of aldehyde functionalities (~41% CHO-Im). Note that comparison of Zn, N and O binding energies for ZIF-8-CHO and bilayer ZIF-8_ZIF-90 shows clear difference, confirming that the nature of functionalization is very different.

Spatial distribution of functionalized linker

To gain further insight into the incorporation of the 2-imidazolecarboxaldehyde (CHO-Im) linker within the ZIF-8 framework, angle-dependent IRRAS was performed (Figure 4a)³⁶. Spectra were collected at three incident angles 35°, 45° and 75°. Analysis of the spectra revealed that the intensity of the peaks at 1325 cm⁻¹ (H–CO stretching), 1200 cm⁻¹ (C–N stretching), and 1168 cm⁻¹ characteristics¹⁹ of ZIF-90 increases

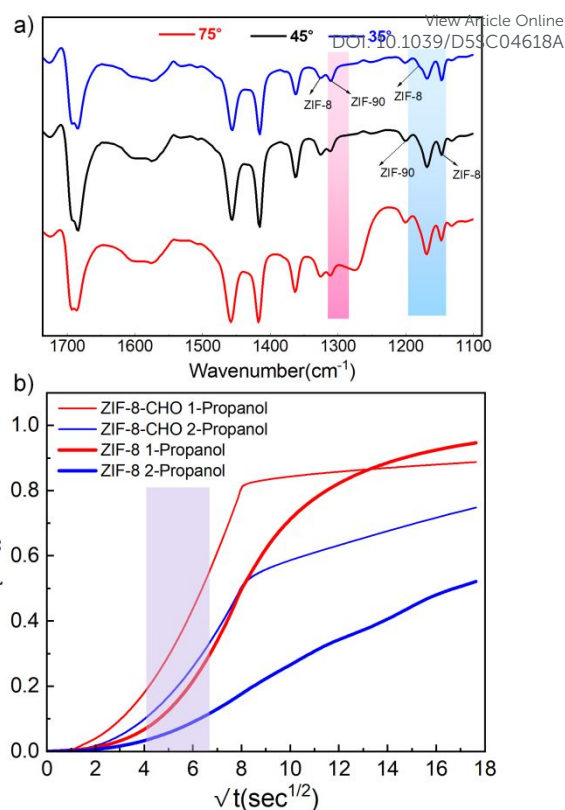


Figure 4. a) Angle dependent IRRAS of ZIF-8-CHO at 35°, 45° and 75°. b) 1-propanol and 2-propanol vapour uptake profiles for the ZIF-8 and ZIF-8-CHO thin film. Shaded region was used for slope calculation.

progressively from 35° to 75°. In contrast, the peaks at 1310 cm⁻¹ and 1146 cm⁻¹, associated with ZIF-8³⁷, show decreasing trend of intensity. This angle-dependent spectral behaviour indicates a compositional gradient within the film, with the CHO-Im linker predominantly incorporated near the surface. We attribute this spatial distribution to the linker vapour diffusion along the film thickness.

To confirm that the functionalization of ZIF-8 with CHO-Im linker is successful, we have performed 1 and 2-propanol vapour uptake measurements on neat ZIF-8 and ZIF-8-CHO thin films. To do so, we have grown both the thin films on Au-coated quartz crystal sensors (see experimental section) and measured the fundamental frequencies under a constant flow of saturated vapours of 1 and 2-propanol^{6, 38, 39}. The uptake profiles are shown in Figure 4b. Comparison of the slopes (at the linear region of the uptake profiles) confirmed that the functionalization of ZIF-8 by CHO-Im reduces the 1-propanol/2-propanol selectivity. This is according to the literature precedence^{40, 41}. Addition of CHO-group reduces the isomer recognition, thereby decreasing the diffusion selectivity.

CO₂/N₂ permselectivity

To investigate the influence of spatial gradient on molecular sieving performance, we have fabricated ZIF-8-CHO and ZIF-8_ZIF-90 membranes on porous anodic alumina oxide (AAO; pore size ~ 100 nm) and compared the CO₂/N₂ permselectivity (Figure 4). The synthesis methodologies were similar to those



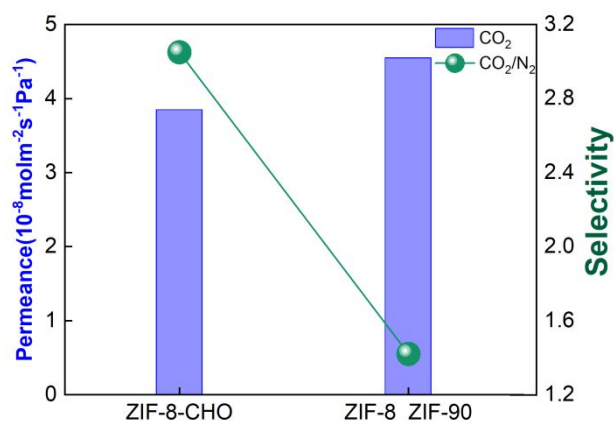


Figure 5. CO₂ permeance and CO₂/N₂ selectivity of the ZIF-8-CHO and ZIF-8_ZIF-90 (CO₂ gas permeance = purple bar, CO₂/N₂ selectivity = green circle)

used for film growth on Au substrate. The continuous film formation was tested by SEM experiments (Figure S3-4). The gas permeation experiments were carried out using a custom made Wicke-Kallenbach setup (Figure S5) at 303 K under a constant transmembrane pressure (4 bar). We have also performed pressure dependent permeance measurements on both of the membranes and realized similar permeance values, confirming the absence of any pinhole (Figure S6). An earlier study on neat ZIF-8 membrane, fabricated using similar methodology as in the current work, exhibited an ideal CO₂/N₂ permselectivity of 2.2 (CO₂ permeance $\sim 9.5(\pm 2) \times 10^{-8} \text{ molm}^{-2}\text{s}^{-1}\text{Pa}^{-1}$)⁴². We observed that in the case of ZIF-8-CHO, the ideal CO₂/N₂ permselectivity was ~ 3 (CO₂ permeance $\sim 3.8(\pm 2) \times 10^{-8} \text{ molm}^{-2}\text{s}^{-1}\text{Pa}^{-1}$). The enhanced selectivity is attributed to the inclusion of -CHO functionality in ZIF-8 lattice, leading to a constricted pore window and specific CO₂-C=O (CHO) interaction. Interestingly, the ZIF-8_ZIF-90 membrane exhibited much lower permselectivity of 1.4 (Figure 4). Hence, it is evident that presence of only ZIF-90 does not enhance the selectivity; rather, the spatial functional gradient in ZIF-8-CHO does enhance the sieving performance. Note that a homogeneously mixed ZIF-8-CHO membrane synthesis was not possible and hence a direct comparison could not be done.

Conclusions

Functional porous solids, like ZIFs, are significant materials for chemical separation. Designing of the pore surface of the ZIFs with multiple chemical functionalities are advantageous in the context of selective adsorption. However, controlling the spatial distribution of the chemical functionalities is rarely achieved. Leveraging vapour phase linker exchange reaction and the diffusion gradient, a spatially gradient functionalized ZIF-8 thin film is realized. We demonstrate that vapor phase reaction yields a functionalized ZIF-8 lattice, and the unique pore environment shows improved gas permselectivity, compared to the pristine MOFs. The findings presented here demonstrate a potential strategy to alter and tune porous thin membranes for advanced separation technology. Also, the

impact of graded spatial distribution needs further study to explore its full potential for chemical separation.

Author Contributions

A.Y and R.H conceived the idea and planned the experiments, A.Y performed the experiments and characterizations, S.K helped with SEM, G.M did the DFT with the guidance of S.G, S.K and G.M contributed equally. manuscript draft was prepared with the inputs from all authors.

Conflicts of interest

There are no conflicts to declare.

Acknowledgements

We acknowledge the financial support from Science and Engineering Research Board (SERB); Govt. of India (Project no: SRG/2022/000927) and intramural funds at TIFR Hyderabad from the Department of Atomic Energy (DAE), India, under Project Identification Number RTI 4007.

References

1. K. S. Park, Z. Ni, A. P. Côté, J. Y. Choi, R. Huang, F. J. Uribe-Romo, H. K. Chae, M. O'Keeffe and O. M. Yaghi, *Proceedings of the National Academy of Sciences*, 2006, **103**, 10186-10191.
2. N. T. T. Nguyen, H. Furukawa, F. Gándara, H. T. Nguyen, K. E. Cordova and O. M. Yaghi, *Angewandte Chemie International Edition*, 2014, **53**, 10645-10648.
3. B. Li, H.-M. Wen, H. Wang, H. Wu, T. Yildirim, W. Zhou and B. Chen, *Energy & Environmental Science*, 2015, **8**, 2504-2511.
4. H. Deng, C. J. Doonan, H. Furukawa, R. B. Ferreira, J. Towne, C. B. Knobler, B. Wang and O. M. Yaghi, *Science*, 2010, **327**, 846-850.
5. S. Zhou, O. Shekhah, A. Ramírez, P. Lyu, E. Abou-Hamad, J. Jia, J. Li, P. M. Bhatt, Z. Huang, H. Jiang, T. Jin, G. Maurin, J. Gascon and M. Eddaoudi, *Nature*, 2022, **606**, 706-712.
6. T. Maity, S. Sarkar, S. Kundu, S. Panda, A. Sarkar, R. Hammad, K. Mandal, S. Ghosh, J. Mondal and R. Halder, *Nature Communications*, 2024, **15**, 9636.
7. J. Jia, L. Gutiérrez-Arzaluz, O. Shekhah, N. Alsadun, J. Czában-Jóźwiak, S. Zhou, O. M. Bakr, O. F. Mohammed and M. Eddaoudi, *Journal of the American Chemical Society*, 2020, **142**, 8580-8584.
8. R. Halder, M. Jakoby, A. Mazel, Q. Zhang, A. Welle, T. Mohamed, P. Krolla, W. Wenzel, S. Diring, F. Odobel, B. S. Richards, I. A. Howard and C. Wöll, *Nature Communications*, 2018, **9**, 4332.
9. M. Oldenburg, A. Turshatov, D. Busko, S. Wollgarten, M. Adams, N. Baroni, A. Welle, E. Redel, C. Wöll, B. S. Richards and I. A. Howard, *Advanced Materials*, 2016, **28**, 8477-8482.



10. Z. Xu, A. Chandresh, A. Mauri, M. Esmaeilpour, V. Monnier, F. Odobel, L. Heinke, W. Wenzel, M. Kozłowska, S. Diring, R. Haldar and C. Wöll, *Angewandte Chemie International Edition*, 2024, **63**, e202414526.
11. Y. Yin, S. Feng, X. Xu, Y. Liu, Y. Li, L. Gao, X. Zhou, J. Dong, Y. Wu, J. Su, J.-L. Zuo, S. Yuan and J. Zhu, *Journal of the American Chemical Society*, 2025, **147**, 16481-16493.
12. M. Mon, R. Bruno, E. Tiburcio, M. Viciano-Chumillas, L. H. G. Kalinke, J. Ferrando-Soria, D. Armentano and E. Pardo, *Journal of the American Chemical Society*, 2019, **141**, 13601-13609.
13. K. Roztocki, M. K. Dudek, M. Szufla, F. Formalik, V. Bon, A. Krawczuk, P. Paluch, S. Kaskel and D. Matoga, *Chemistry of Materials*, 2024, **36**, 8578-8587.
14. X. Kong, H. Deng, F. Yan, J. Kim, J. A. Swisher, B. Smit, O. M. Yaghi and J. A. Reimer, *Science*, 2013, **341**, 882-885.
15. S. Jeong, J. Seong, S. W. Moon, J. Lim, S. B. Baek, S. K. Min and M. S. Lah, *Nature Communications*, 2022, **13**, 1027.
16. Z. Zheng, Z. Rong, H. L. Nguyen and O. M. Yaghi, *Inorganic Chemistry*, 2023, **62**, 20861-20873.
17. A. Phan, C. J. Doonan, F. J. Uribe-Romo, C. B. Knobler, M. O'Keeffe and O. M. Yaghi, *Accounts of Chemical Research*, 2010, **43**, 58-67.
18. R. Banerjee, A. Phan, B. Wang, C. Knobler, H. Furukawa, M. O'Keeffe and O. M. Yaghi, *Science*, 2008, **319**, 939-943.
19. K. Eum, K. C. Jayachandrababu, F. Rashidi, K. Zhang, J. Leisen, S. Graham, R. P. Lively, R. R. Chance, D. S. Sholl, C. W. Jones and S. Nair, *Journal of the American Chemical Society*, 2015, **137**, 4191-4197.
20. J. A. Thompson, C. R. Blad, N. A. Brunelli, M. E. Lydon, R. P. Lively, C. W. Jones and S. Nair, *Chemistry of Materials*, 2012, **24**, 1930-1936.
21. J. A. Thompson, N. A. Brunelli, R. P. Lively, J. R. Johnson, C. W. Jones and S. Nair, *The Journal of Physical Chemistry C*, 2013, **117**, 8198-8207.
22. Q. T. Nguyen, J. Y. Lee, Y. Bae, Y.-R. Lee, Y. Song, S. H. Kim, K.-Y. Baek and J. Na, *ChemSusChem*, 2025, **18**, e202401968.
23. W. Wu, J. Su, M. Jia, Z. Li, G. Liu and W. Li, *Science Advances*, 2020, **6**, eaax7270.
24. P. Su, M. Tu, R. Ameloot and W. Li, *Accounts of Chemical Research*, 2022, **55**, 186-196.
25. L. Xue, G. Luo, X.-c. Yang, Y. Qin and B. Zhang, *The Innovation Materials*, 2024, **2**, 100047.
26. J. Marreiros, L. Van Dommelen, G. Fleury, R. de Oliveira-Silva, T. Stassin, P. Iacomini, S. Furukawa, D. Sakellariou, P. L. Llewellyn, M. Roefsaers and R. Ameloot, *Angewandte Chemie International Edition*, 2019, **58**, 18471-18475.
27. Q. Hou, Y. Wu, S. Zhou, Y. Wei, J. Caro and H. Wang, *Angewandte Chemie International Edition*, 2019, **58**, 327-331.
28. S. Berens, F. Hillman, H.-K. Jeong and S. Vasenkov, *Microporous and Mesoporous Materials*, 2019, **288**, 109603.
29. M. Åhlén, A. Jaworski, M. Strømme and O. Cheung, *Chemical Engineering Journal*, 2021, **422**, 130117.
30. W.-L. Xue, P. Kolodzeiski, H. Aucharova, S. Vasa, A. Koutsianos, R. Pallach, J. Song, L. Frentzel-Beyme, R. Linser and S. Henke, *Nature Communications*, 2024, **15**, 4420.
31. Y. Pan, D. Heryadi, F. Zhou, L. Zhao, G. Lestari, H. Su and Z. Lai, *CrystEngComm*, 2011, **13**, 6937-6940.
32. J. A. Boissonnault, A. G. Wong-Foy and A. J. Matzger, *Journal of the American Chemical Society*, 2017, **139**, 14841-14844.
33. R. Ahmad, U. A. Khan, N. Iqbal and T. Noor, *RSC Advances*, 2020, **10**, 43733-43750.
34. Y. Wang, Y. Wang, L. Zhang, C.-S. Liu and H. Pang, *Inorganic Chemistry Frontiers*, 2019, **6**, 2514-2520.
35. E. P. Valadez Sánchez, H. Gliemann, K. Haas-Santo, C. Wöll and R. Dittmeyer, *Chemie Ingenieur Technik*, 2016, **88**, 1798-1805.
36. S. Panda, S. Kundu, P. Malik and R. Haldar, *Chemical Science*, 2024, **15**, 2586-2592.
37. M. Ahmad, R. Patel, D. T. Lee, P. Corkery, A. Kraetz, Prerna, S. A. Tenney, D. Nykypanchuk, X. Tong, J. I. Siepmann, M. Tsapatsis and J. A. Boscoboinik, *ACS Applied Materials & Interfaces*, 2024, **16**, 27887-27897.
38. P. Malik and R. Haldar, *Molecular Systems Design & Engineering*, 2022, **7**, 873-877.
39. S. Panda, T. Maity, S. Sarkar, A. K. Manna, J. Mondal and R. Haldar, *Nature Communications*, 2025, **16**, 1231.
40. K. Zhang, R. P. Lively, M. E. Dose, A. J. Brown, C. Zhang, J. Chung, S. Nair, W. J. Koros and R. R. Chance, *Chemical Communications*, 2013, **49**, 3245-3247.
41. O. Zybaylo, O. Shekhah, H. Wang, M. Tafipolsky, R. Schmid, D. Johannsmann and C. Wöll, *Physical Chemistry Chemical Physics*, 2010, **12**, 8093-8098.
42. S. Kundu, T. Maity, S. Panda and R. Haldar, *Chemistry – A European Journal*, 2024, **30**, e202403607.



All the data is available upon request to the corresponding author.

[View Article Online](#)
DOI: 10.1039/D5SC04618A

